



THE UNIVERSITY *of* EDINBURGH

Edinburgh Research Explorer

An evolutionarily conserved ribosome-rescue pathway maintains epidermal homeostasis

Citation for published version:

Liakath-Ali, K, Mills, EW, Sequeira, I, Lichtenberger, BM, Pisco, AO, Sipilä, KH, Mishra, A, Yoshikawa, H, Wu, CC-C, Ly, T, Lamond, AI, Adham, IM, Green, R & Watt, FM 2018, 'An evolutionarily conserved ribosome-rescue pathway maintains epidermal homeostasis', *Nature*, vol. 556, pp. 376–380.
<https://doi.org/10.1038/s41586-018-0032-3>

Digital Object Identifier (DOI):

[10.1038/s41586-018-0032-3](https://doi.org/10.1038/s41586-018-0032-3)

Link:

[Link to publication record in Edinburgh Research Explorer](#)

Document Version:

Peer reviewed version

Published In:

Nature

General rights

Copyright for the publications made accessible via the Edinburgh Research Explorer is retained by the author(s) and / or other copyright owners and it is a condition of accessing these publications that users recognise and abide by the legal requirements associated with these rights.

Take down policy

The University of Edinburgh has made every reasonable effort to ensure that Edinburgh Research Explorer content complies with UK legislation. If you believe that the public display of this file breaches copyright please contact openaccess@ed.ac.uk providing details, and we will remove access to the work immediately and investigate your claim.



1 **An evolutionarily conserved ribosome-rescue pathway maintains epidermal homeostasis**

2
3 Kifayathullah Liakath-Ali^{1, #}, Eric W. Mills², Inês Sequeira¹, Beate M. Lichtenberger^{1, 3}, Angela
4 Oliveira Pisco¹, Kalle H. Sipilä¹, Ajay Mishra^{1,4}, Harunori Yoshikawa⁵, Colin Chih-Chien Wu²,
5 Tony Ly^{5,6}, Angus I Lamond⁶, Ibrahim M. Adham⁷, Rachel Green² and Fiona M. Watt¹

- 6
7 1. Centre for Stem Cells and Regenerative Medicine, King's College London, 28th floor,
8 Guy's Tower Wing, London SE1 9RT, UK.
9 2. Howard Hughes Medical Institute, Johns Hopkins School of Medicine, Department of
10 Molecular Biology and Genetics, Baltimore, MD 21205, USA.
11 3. Skin & Endothelium Research Division, Department of Dermatology, Medical University
12 of Vienna, Lazarettgasse 14, 1090 Vienna, Austria
13 4. Cambridge Infinitus Research Centre, University of Cambridge, Cambridge, UK
14 5. Centre for Gene Regulation and Expression, School of Life Sciences, University of
15 Dundee, Dow Street, Dundee, DD1 5EH, Scotland, UK.
16 6. Wellcome Trust Centre for Cell Biology, University of Edinburgh, Michael Swann
17 Building, King's Buildings, Edinburgh EH9 3BF, Scotland, UK.
18 7. Institute of Human Genetics, University Medical Centre of Göttingen, D-37073
19 Göttingen, Germany.

20 # Present address: Department of Molecular and Cellular Physiology and Howard Hughes
21 Medical Institute, Stanford University Medical School, 265 Campus Drive, CA 94305-
22 5453, USA

23
24 Address for communication: fiona.watt@kcl.ac.uk

29 **Ribosome-associated mRNA quality control mechanisms ensure fidelity of protein**
30 **translation^{1,2}. Although extensively studied in yeast, little is known about their role in**
31 **mammalian tissues, despite emerging evidence that stem cell fate is controlled by**
32 **translational mechanisms^{3,4}. One evolutionarily conserved component of the quality control**
33 **machinery, *Dom34/Pelota (Pelo)*, rescues stalled ribosomes⁵. Here we show that *Pelo* is**
34 **required for mammalian epidermal homeostasis. Conditional deletion of *Pelo* in those**
35 **murine epidermal stem cells that express *Lrig1* results in hyperproliferation and abnormal**
36 **differentiation. In contrast, deletion in *Lgr5*+ stem cells has no effect and deletion in *Lgr6*+**
37 **stem cells has only a mild phenotype. Loss of *Pelo* results in accumulation of short**
38 **ribosome footprints and global upregulation of translation rather than affecting expression**
39 **of specific genes. Translational inhibition by rapamycin-mediated down regulation of**
40 **mTOR rescues the epidermal phenotype. Our study reveals a novel role for the ribosome-**
41 **rescue machinery in mammalian tissue homeostasis and an unanticipated specificity in its**
42 **impact on different stem cell populations.**

43 *Pelo* is expressed in mouse skin dermis and epidermis⁶ (Extended Data Fig. 1a). Dermal-specific
44 deletion (*Pelo*^{derKO}) resulted in mice that were smaller than littermate controls but had a normal
45 lifespan and no dermal abnormalities (Fig. 1a-f). Although Dom34 forms a functional complex
46 with Hbs1 in yeast⁷ and the mammalian homolog *Hbs1l* is expressed in mouse skin⁶ (Extended
47 Data Fig. 1b), the *Hbs1l* knockout (from exon 5; Extended Data Fig. 1c) had no epidermal
48 defects (Extended Data Fig. 1d-f) and only small changes in dermal collagen deposition,
49 thickness and cell density (Extended Data Fig. 1f-m). Another *Pelo* partner, *Gtpbp2*⁸, does not
50 have a reported skin phenotype.

51 Selective embryonic deletion of *Pelo* in Krt14 expressing epidermal cells, comprising the known
52 stem cell subpopulations⁹, via *Krt14*^{Cre} (*Pelo*^{epiKO}; Fig. 1g) phenocopied deletion via the
53 ubiquitous Rosa26 locus¹⁰. Mice were born with scaly skin and an epidermal barrier defect
54 (increased trans epidermal water loss; TEWL). They exhibited hair and weight loss, failing to
55 thrive beyond 5 months (Fig. 1h-k). Epidermal thickening resulted from increased proliferation
56 (Fig. 1l-q) and abnormal accumulation of differentiated cells (Fig. 1n-t). Wound closure was
57 delayed (Fig. 1u), correlating with reduced proliferation, differentiation and migration (Extended
58 Data Fig. 2a-i). Hyperproliferation in unwounded skin combined with delayed wound healing
59 and abnormal differentiation has been observed in other mouse models¹¹. There was also striking
60 degeneration of the sebaceous glands and hair follicles, correlating with loss of the hair follicle
61 bulge stem cell markers Krt15 and CD34 and the junctional zone stem cell marker Lrig1
62 (Extended Data Fig. 3a-c).

63

64 To determine whether the *Pelo* epidermal phenotype could be induced postnatally, we applied 4-
65 OHT to adult *Pelo*^{fl/fl}; *Krt14*^{CreERT} (Extended Data Fig. 4a, b). Mice developed skin lesions,
66 increased TEWL and delayed wound closure (Extended Data Fig. 4c-e). Degeneration of hair
67 follicles and sebaceous glands correlated with keratinized cyst formation (Extended Data Fig. 4f,
68 g). Sebocyte differentiation was disturbed, accompanied by expansion of Lrig1 labelling into the
69 upper sebaceous gland (Extended Data Fig. 4h, i).

70

71 *PELO* knockdown in cultured human epidermal keratinocytes led to an increase in stem cell
72 colonies (Extended Data Fig. 5a-g). Immunostaining of epidermis reconstituted on decellularised
73 dermis revealed increased proliferation of basal layer cells and increased differentiated layers

74 (Extended Data Fig. 5h-l). Therefore the mouse epidermal *Pelo* phenotype was recapitulated in
75 human cells.

76

77 To determine if there is a differential requirement for *Pelo* in different epidermal subpopulations,
78 we conditionally deleted *Pelo* in *Lgr5*⁺, *Lgr6*⁺ and *Lrig1*⁺ stem cells (Fig. 2a-c). *Pelo* deletion in
79 *Lrig1*⁺ cells recapitulated the effects of deleting *Pelo* in *Krt14*⁺ cells, whereas when *Pelo* was
80 deleted in *Lgr5*⁺ and *Lgr6*⁺ cells differentiation was normal (Fig. 2d) with only a small increase
81 in *Ki67*⁺ cells (Extended Data Fig. 5m, Fig. 2f). *Pelo* deletion in *Lrig1*⁺ cells increased cell
82 proliferation in the upper hair follicle, with marked changes in follicles and sebaceous glands
83 (Fig. 2e, Extended Data Fig. 6a, b). A significant increase in proliferation and TEWL occurred in
84 the interfollicular epidermis (IFE) of *Pelo*^{fl/fl}; *Lrig1*^{CreERT2} mice compared to *Pelo*^{fl/fl}; *Lgr5*^{CreERT2}
85 and *Pelo*^{fl/fl}; *Lgr6*^{CreERT2} mice (Extended Data Fig.5m, Fig. 2f, h). There was a small increase in
86 epidermal thickness in *Pelo*^{fl/fl}; *Lgr6*^{CreERT2} mice but TEWL was unaffected (Fig. 2g, h).

87

88 We next generated *Pelo*^{fl/fl}; *Lrig1*^{CreERT2}; *Rosa26*^{tdTom}, *Pelo*^{fl/fl}; *Lgr5*^{CreERT2}; *Rosa26*^{tdTom}, and
89 *Pelo*^{fl/fl}; *Lgr6*^{CreERT2}; *Rosa26*^{tdTom} mice, and treated with 4-OHT. *Pelo* deletion did not change the
90 contribution of *Lgr5* or *Lgr6* progeny to the epidermis (Extended Data Fig. 6c, d). In contrast, on
91 *Pelo* deletion *Lrig1* lineage cells expanded downwards into the hair follicles and fully colonized
92 the IFE (Extended Data Fig. 6c, d). In the presence or absence of *Pelo*, the *Lrig1* lineage
93 accounted for most *Ki67*⁺ epidermal cells; they also accounted for the increase in proliferative
94 cells on *Pelo* deletion (Extended Data Fig. 6e, f).

95

96 Yeast cells lacking *Dom34* (the homolog of *Pelo*) are enriched in short 16-18 nucleotide
97 ribosome-protected fragments (RPFs) resulting from translation to the 3' end of truncated
98 mRNAs⁵. *Dom34/Rli1* mutant yeast accumulate full length 28-32 nucleotide RPFs in 3' UTRs,
99 consistent with the role of *Dom34* and *Rli1* in ribosome rescue and recycling on intact mRNAs,
100 respectively¹². In anucleate hematopoietic cells PELO and ABCE1 (*Rli1*) rescue non-translating
101 3'UTR ribosomes¹³ and impact mRNA stability¹⁴. When we performed ribosomal profiling on
102 keratinocytes from adult *Pelo*^{epiKO} mice by deep sequencing RPFs¹⁵, RPFs mapped primarily to
103 the coding sequence (CDS) (Fig. 3a; Extended Data Fig. 7a, b), consistent with studies¹² showing
104 that loss of PELO alone does not substantially increase 3' UTR ribosomes. CDS RPFs were
105 primarily 28-34nts, the expected fragment size protected by mammalian ribosomes¹⁶, and
106 displayed the three-nucleotide periodicity reflecting codon-by-codon movement of elongating
107 ribosomes (Fig. 3b, gray bars).

108

109 *Pelo*^{epiKO} profiles were enriched in 20-21 nucleotide RPFs (~4-5% of total RPFs compared to
110 <1% in control cells) (Fig. 3a-c). Like the dominant population of 28-34nt RPFs, these footprints
111 were primarily found in the CDS and showed a strong reading frame signal, indicating they too
112 reflect the presence of elongating ribosomes, yet are shortened on their 3' end after nuclease
113 digestion (Fig. 3d, right). The density of short RPFs was evenly distributed and did not increase
114 in frequency near the downstream 3' portion of transcripts (Fig. 3a), as would be anticipated if
115 they resulted from ribosomes encountering a directional RNA decay process^{17,18}. Consistent with
116 this, enrichment for 20-21 nt footprints was not linked to reduced transcript abundance in
117 *Pelo*^{epiKO} cells (Fig. 3e; Supplementary Table 1). While *Pelo* is implicated in decay of the
118 unusual histone mRNAs that lack polyA tails¹⁹, the short footprints did not demonstrate patterns

119 to indicate they result from ribosomes occupying transcripts that are being degraded. The 21mer
120 RPFs seen in *Pelo*^{epiKO} cells could be the equivalent of the 16mer species in yeast⁵ and reflect the
121 increased size of the mammalian ribosome²⁰. However, we suggest they are equivalent to the
122 21nt fragments observed²¹ in anisomycin-treated yeast cells and reflect dependence on *Pelo*-
123 associated quality control mechanisms in response to tRNA starvation in rapidly dividing cells.

124

125 Epidermal *Pelo* loss led to significant changes in global translational efficiency (TE)¹⁵ (Fig. 3f,
126 g; $p < 0.01$). TE values for keratins and ribosomal proteins were notably increased (Fig. 3f, g).
127 There was significant enrichment for genes involved in RNA metabolism, protein synthesis,
128 extracellular matrix and chromatin regulation (Fig. 3h; Extended Data Fig. 7c to e;
129 Supplementary Table 2; Supplementary Table 3). There was also differential expression of
130 canonical translational pathways, including upregulation of the mTOR (mechanistic target of
131 rapamycin) pathway (Fig. 3h; Extended Data Fig. 8a, b). Since mTOR signaling leads to
132 increased global translation²² (Extended Data Fig. 8c), we compared the *Gtpbp2*/tRNA mutant⁸
133 and *Pelo*^{epiKO} gene expression datasets. We found significant overlap in translational signaling
134 pathways (Extended Data Fig. 8d), suggesting that ribosome stalling is sensed by mTOR.

135

136 The polysome-to-monosome ratio was increased in *Pelo*^{epiKO} cells (Fig. 3i), suggesting an overall
137 increase in translation or accumulation of inactive stalled ribosomes. *Krt86* transcripts were
138 enriched in the heavy polysome fractions (Fig. 3j), consistent with the increases in TE values,
139 suggesting increased overall translation. This was confirmed by quantifying global protein
140 synthesis by O-propargyl-puromycin (OP-P) incorporation into newly synthesized polypeptide
141 chains^{3,4}. OP-P incorporation was increased in *Pelo*^{epiKO} IFE and hair follicles compared to

142 controls. Labelling was higher in the IFE suprabasal than basal layer, consistent with increased
143 total protein synthesis during differentiation (Fig. 4a-d)²³. The increase in OP-P labelling in total
144 *Pelo* null keratinocytes (Fig. 4e) and stem cells (Integrin α 6-high cells; Itga6^{high}) was confirmed
145 by flow cytometry (Extended Data Fig. 9a, Fig. 4f-j). Confocal microscopy revealed a striking
146 increase in the size of *Pelo*^{epiKO} basal cells (Extended Data Fig. 9b-d), consistent with increased
147 protein synthesis and a higher proportion of G2/M and S phase cells (Extended Data Fig. 9e).

148

149 In control mice, Lrig1+ cells exhibited slightly higher protein synthesis than Lgr5 and Lgr6+
150 cells (Fig. 4k, l). When *Pelo* was deleted, protein synthesis in Lrig1+ cells was increased further
151 relative to Lgr5 and Lgr6+ cells (Fig. 4k, l). RNA-seq (Extended Data Fig. 10a) revealed that
152 regardless of whether or not *Pelo* was expressed, Lgr5+ cells clustered separately from Lrig1+
153 and Lgr6+ cells, while the gene expression profiles of individual populations did not cluster
154 based on *Pelo* expression (Extended Data Fig. 10b-j, Supplementary Tables 4, 5). Therefore the
155 *Pelo* epidermal phenotype primarily reflects increased translation, rather than expression of
156 specific genes.

157

158 To down regulate mTOR1²², we applied rapamycin to adult *Pelo*^{epiKO} skin (Extended Data Fig.
159 9f, g). There was a significant reduction in Ki67+ cells compared to controls (Extended Data Fig.
160 9h-j). Phosphorylated ribosomal protein S6K (pS6K), a key substrate of mTOR²², was increased
161 in *Pelo*^{epiKO} skin, and reduced by rapamycin (Extended Data Fig. 9k). However, rapamycin did
162 not prevent disruption of hair follicle and sebaceous gland architecture (Extended Data Fig. 9h).

163

164 Simultaneous rapamycin treatment and *Pelo* deletion largely prevented *Pelo*-mediated disruption
165 of epidermal homeostasis (Fig. 4m, n). TEWL, epidermal thickening and proliferation were
166 substantially reduced (Fig. 4o-u; Extended Data Fig. 9l); pS6K labeling was reduced (Fig. 4v)
167 and phosphorylation of another mTOR substrate, 4EBP1, was decreased (Extended Data Fig.
168 9m). Therefore the epidermal *Pelo* deletion phenotype is largely attributable to increased protein
169 translation.

170

171 Our results indicate that translational control is critical for tissue homeostasis^{3,4,13} and establish a
172 link between *Pelo* inactivation and translational activation via mTOR. mTOR is known to
173 regulate cell growth and proliferation^{22,24} and is activated upon ribosome-stalling by Fragile X
174 Mental Retardation Protein^{25,26}. Impaired ribosomal biogenesis also activates mTOR1 signaling
175 and stimulates translation initiation and elongation factors²⁷. mTOR signaling may be activated
176 to enhance the efficiency of the translational machinery in order to compensate for impaired or
177 reduced availability of ribosomes^{8,28}.

178

179 The increased size of *Pelo*-null epidermal cells as a result of increased protein synthesis^{23,30} may
180 stimulate differentiation through decreased basement membrane engagement²⁹ and thus
181 indirectly promote proliferation. Factors that may account for the selective sensitivity of Lrig1+
182 cells to *Pelo* deletion, include their proliferative state, abundance and location relative to Lgr5+
183 and Lgr6+ cells, together with their known ability to repopulate different epidermal
184 compartments³¹.

185

186

187 **Acknowledgements**

188 We dedicate this work to Wolfgang Engel. FMW gratefully acknowledges funding from the
189 Wellcome Trust and UK Medical Research Council. We are also grateful for funding from the
190 Department of Health via the National Institute for Health Research comprehensive Biomedical
191 Research Centre award to Guy's & St Thomas' National Health Service Foundation Trust in
192 partnership with King's College London and King's College Hospital NHS Foundation Trust.
193 RG acknowledges funding from Howard Hughes Medical Institute. We thank Dr. Christopher
194 Lelliott and Valerie Vancollie for providing *Hbs1l* knockout samples, Drs. Benedicte Oules for
195 critical reading of the manuscript, Drs. D. V. Krishna Pantakani, Aamir Ahmed, Shukry Habib,
196 Ignacio Sancho-Martinez, Giacomo Donati, Magnus Lynch and all Wattlelab members for helpful
197 discussions. Technical help from Mr. Chaozheng Li, Mr. Matteo Battilocchi and staff at the
198 Nikon Imaging Centre and the Hodgkin Biological Services Facility, King's College London is
199 gratefully acknowledged. We thank the High-Throughput Genomics Group at the Wellcome
200 Trust Centre for Human Genetics (funded by Wellcome Trust: 203141/Z/16/Z) for generation of
201 the sequencing data.

202

203 **Author contributions**

204 KL and FMW conceptualized the study. KL, IS and BML performed and analysed mouse
205 experiments. KHS and AJ performed and analysed cell culture experiments. AOP analysed data
206 from ribosome profile and RNA-seq experiments. IMA generated the *Pelo* conditional knockout
207 mouse. EWM, CCW and RG generated and analysed ribosome-profiling data. HY, TL and AIL
208 generated and analyzed polysome data. KL and FMW wrote the manuscript with input from all
209 authors.

210 **Author Information**

211 Authors declare no competing financial interests. Correspondence and requests should be
212 addressed to Fiona Watt (Fiona.watt@kcl.ac.uk).

213

214 **References**

- 215 1 Brandman, O. & Hegde, R. S. Ribosome-associated protein quality control. *Nat Struct*
216 *Mol Biol* **23**, 7-15, doi:10.1038/nsmb.3147 (2016).
- 217 2 Shoemaker, C. J. & Green, R. Translation drives mRNA quality control. *Nat Struct Mol*
218 *Biol* **19**, 594-601, doi:10.1038/nsmb.2301 (2012).
- 219 3 Blanco, S. *et al.* Stem cell function and stress response are controlled by protein
220 synthesis. *Nature* **534**, 335-340, doi:10.1038/nature18282 (2016).
- 221 4 Signer, R. A., Magee, J. A., Salic, A. & Morrison, S. J. Haematopoietic stem cells require
222 a highly regulated protein synthesis rate. *Nature* **509**, 49-54, doi:10.1038/nature13035
223 (2014).
- 224 5 Guydosh, N. R. & Green, R. Dom34 rescues ribosomes in 3' untranslated regions. *Cell*
225 **156**, 950-962, doi:10.1016/j.cell.2014.02.006 (2014).
- 226 6 Rezza, A. *et al.* Signaling Networks among Stem Cell Precursors, Transit-Amplifying
227 Progenitors, and their Niche in Developing Hair Follicles. *Cell Rep* **14**, 3001-3018,
228 doi:10.1016/j.celrep.2016.02.078 (2016).
- 229 7 Becker, T. *et al.* Structure of the no-go mRNA decay complex Dom34-Hbs1 bound to a
230 stalled 80S ribosome. *Nat Struct Mol Biol* **18**, 715-720, doi:10.1038/nsmb.2057 (2011).
- 231 8 Ishimura, R. *et al.* RNA function. Ribosome stalling induced by mutation of a CNS-
232 specific tRNA causes neurodegeneration. *Science* **345**, 455-459,
233 doi:10.1126/science.1249749 (2014).
- 234 9 Kretschmar, K., Weber, C., Driskell, R. R., Calonje, E. & Watt, F. M.
235 Compartmentalized Epidermal Activation of beta-Catenin Differentially Affects Lineage
236 Reprogramming and Underlies Tumor Heterogeneity. *Cell Rep* **14**, 269-281,
237 doi:10.1016/j.celrep.2015.12.041 (2016).
- 238 10 Elkenani, M. *et al.* Pelota Regulates Epidermal Differentiation by Modulating BMP and
239 PI3K/AKT Signaling Pathways. *J Invest Dermatol* **136**, 1664-1671,
240 doi:10.1016/j.jid.2016.04.020 (2016).
- 241 11 Florin, L. *et al.* Delayed wound healing and epidermal hyperproliferation in mice lacking
242 JunB in the skin. *J Invest Dermatol* **126**, 902-911, doi:10.1038/sj.jid.5700123 (2006).
- 243 12 Young, D. J., Guydosh, N. R., Zhang, F., Hinnebusch, A. G. & Green, R. Rli1/ABCE1
244 Recycles Terminating Ribosomes and Controls Translation Reinitiation in 3'UTRs In
245 Vivo. *Cell* **162**, 872-884, doi:10.1016/j.cell.2015.07.041 (2015).
- 246 13 Mills, E. W., Wangen, J., Green, R. & Ingolia, N. T. Dynamic Regulation of a Ribosome
247 Rescue Pathway in Erythroid Cells and Platelets. *Cell Rep* **17**, 1-10,
248 doi:10.1016/j.celrep.2016.08.088 (2016).
- 249 14 Mills, E. W., Green, R. & Ingolia, N. T. Slowed decay of mRNAs enhances platelet
250 specific translation. *Blood* **129**, e38-e48, doi:10.1182/blood-2016-08-736108 (2017).

251 15 Ingolia, N. T., Brar, G. A., Rouskin, S., McGeachy, A. M. & Weissman, J. S. The
252 ribosome profiling strategy for monitoring translation in vivo by deep sequencing of
253 ribosome-protected mRNA fragments. *Nat Protoc* **7**, 1534-1550,
254 doi:10.1038/nprot.2012.086 (2012).

255 16 Ingolia, N. T., Lareau, L. F. & Weissman, J. S. Ribosome profiling of mouse embryonic
256 stem cells reveals the complexity and dynamics of mammalian proteomes. *Cell* **147**, 789-
257 802, doi:10.1016/j.cell.2011.10.002 (2011).

258 17 Guydosh, N. R., Kimmig, P., Walter, P. & Green, R. Regulated Ire1-dependent mRNA
259 decay requires no-go mRNA degradation to maintain endoplasmic reticulum homeostasis
260 in *S. pombe*. *Elife* **6**, doi:10.7554/eLife.29216 (2017).

261 18 Guydosh, N. R. & Green, R. Translation of poly(A) tails leads to precise mRNA
262 cleavage. *RNA* **23**, 749-761, doi:10.1261/rna.060418.116 (2017).

263 19 Slevin, M. K. *et al.* Deep sequencing shows multiple oligouridylations are required for 3'
264 to 5' degradation of histone mRNAs on polyribosomes. *Mol Cell* **53**, 1020-1030,
265 doi:10.1016/j.molcel.2014.02.027 (2014).

266 20 Ben-Shem, A., Jenner, L., Yusupova, G. & Yusupov, M. Crystal structure of the
267 eukaryotic ribosome. *Science* **330**, 1203-1209, doi:10.1126/science.1194294 (2010).

268 21 Lareau, L. F., Hite, D. H., Hogan, G. J. & Brown, P. O. Distinct stages of the translation
269 elongation cycle revealed by sequencing ribosome-protected mRNA fragments. *Elife* **3**,
270 e01257, doi:10.7554/eLife.01257 (2014).

271 22 Thoreen, C. C. *et al.* A unifying model for mTORC1-mediated regulation of mRNA
272 translation. *Nature* **485**, 109-113, doi:10.1038/nature11083 (2012).

273 23 Kristensen, A. R., Gsponer, J. & Foster, L. J. Protein synthesis rate is the predominant
274 regulator of protein expression during differentiation. *Mol Syst Biol* **9**, 689,
275 doi:10.1038/msb.2013.47 (2013).

276 24 Laplante, M. & Sabatini, D. M. mTOR signaling in growth control and disease. *Cell* **149**,
277 274-293, doi:10.1016/j.cell.2012.03.017 (2012).

278 25 Darnell, J. C. *et al.* FMRP stalls ribosomal translocation on mRNAs linked to synaptic
279 function and autism. *Cell* **146**, 247-261, doi:10.1016/j.cell.2011.06.013 (2011).

280 26 Sawicka, K., Pyronneau, A., Chao, M., Bennett, M. V. & Zukin, R. S. Elevated ERK/p90
281 ribosomal S6 kinase activity underlies audiogenic seizure susceptibility in fragile X mice.
282 *Proc Natl Acad Sci U S A* **113**, E6290-E6297, doi:10.1073/pnas.1610812113 (2016).

283 27 Liu, R. *et al.* Impairing the production of ribosomal RNA activates mammalian target of
284 rapamycin complex 1 signalling and downstream translation factors. *Nucleic Acids Res*
285 **42**, 5083-5096, doi:10.1093/nar/gku130 (2014).

286 28 Mills, E. W. & Green, R. Ribosomopathies: There's strength in numbers. *Science* **358**,
287 doi:10.1126/science.aan2755 (2017).

288 29 Watt, F. M., Jordan, P. W. & O'Neill, C. H. Cell shape controls terminal differentiation of
289 human epidermal keratinocytes. *Proc Natl Acad Sci U S A* **85**, 5576-5580 (1988).

290 30 Gingold, H. *et al.* A dual program for translation regulation in cellular proliferation and
291 differentiation. *Cell* **158**, 1281-1292, doi:10.1016/j.cell.2014.08.011 (2014).

292 31 Page, M. E., Lombard, P., Ng, F., Gottgens, B. & Jensen, K. B. The epidermis comprises
293 autonomous compartments maintained by distinct stem cell populations. *Cell Stem Cell*
294 **13**, 471-482, doi:10.1016/j.stem.2013.07.010 (2013).

295
296
297

298 **Methods**
299

300 **Mouse strains**

301 All mouse experiments were performed under a UK Government Home Office project license
302 and subject to local institutional ethical approval. The generation of conditional *Pelo*^{fl/fl}
303 (*Pelo*^{tm1Imad}) mice was described elsewhere³². To derive constitutive *Pelo* epidermal knockout
304 mice (*Pelo*^{epiKO}), *Pelo*^{fl/fl} mice were crossed with *Krt14*^{Cre} mice (Jax strain, stock number
305 004782). To achieve temporally controlled *Pelo* knockout and genetic labeling of cells lacking
306 *Pelo*, *Pelo*^{fl/fl} mice were crossed with *Krt14*^{CreERT} (Jax strain, stock number 005107), *Lrig1*^{EGFP-}
307 IRES-CreERT2 mice³¹, *Lgr5*^{EGFP-IRES-CreERT2} mice³³, *Lgr6*^{EGFP-IRES-CreERT2} mice³⁴ and *Rosa26*^{LoxP-Stop-}
308 LoxP-tdTomato mice³⁵. To activate Cre recombinase, 4-Hydroxytamoxifen (4-OHT, Sigma-Aldrich)
309 was dissolved in acetone and applied topically (3 mg/100 µl) every day for five days and once a
310 week for three weeks. For proliferation assays, 5-ethynyl-2'-deoxyuridine (EdU) (Invitrogen, 20
311 mg kg⁻¹ body mass; in PBS) was injected intraperitoneally and the tissue was harvested 1 hr
312 later. To derive constitutive *Pelo* dermal knockout mice (*Pelo*^{derKO}), *Pelo*^{fl/fl} mice was crossed
313 with *Dermo1*^{Cre} (B6.129X1-*Twist2*^{tm1.1(cre)Dor/J})^{36,37}. Mouse lines used in this study with the
314 location of expression of markers in the skin are illustrated in the Extended Data Fig. 10k.
315 *Hbs1l*^{-/-} (*Hbs1l*^{tm1a(KOMP)Wtsi}) mice were produced at the Wellcome Trust Sanger Institute Mouse
316 Genetics Project as part of International Mouse Phenotype Consortium (IMPC)³⁸.

317 **Library generation for ribosome profiling**

318 Samples of *Pelo*^{epiKO} epidermis for ribosome profiling and RNA-Seq were prepared by scrapping
319 off the epidermal layer in liquid nitrogen. Frozen samples were ground using a Mixer Mill
320 (Retch) and thawed in the presence of polysome lysis buffer. Lysates were clarified by

321 centrifugation at 20,000g for 10 minutes at 4°C and the supernatant was collected. Total lysate
322 RNA was quantified using the Quant-it RNA kit (Thermo) and 5 µg was used for preparation of
323 ribosome profiling libraries as described previously¹⁵. Total RNA was size-selected by excising
324 gel regions between phosphorylated 16nt and 34nt RNA oligo standards. Ribosomal RNAs were
325 depleted using Ribo-Zero Gold (Illumina) after footprint size-selection. 100ng was used for
326 preparation of RNA-Sequencing libraries from the same samples as profiling libraries. Analysis
327 using a BioAnalyzer total RNA pico chip was used to confirm RNA integrity (RIN >9) for RNA
328 sequencing samples. The datasets are deposited in GEO under accession number GSE94385.

329

330 **Sequencing and data analysis**

331 Ribosome profiling and RNA-Seq libraries were sequenced using a HiSeq2500 (Illumina). ~110
332 million total raw reads were generated from 4 ribosome profiling samples with between 11 and
333 30 million reads mapping to the genome per sample. For ribosome profiling analysis, only
334 singly-mapped reads (NH:i:1) with no mismatches (NM:I:0) were used. Translational efficiency
335 (TE) was calculated as number of CDS RPFs / RPKM. Relative 3'UTR ribosome occupancy was
336 calculated as 3'UTR footprint density / CDS footprint density. For differential gene expression
337 analysis, we uploaded the list of differentially expressed genes into Ingenuity IPA and ran a core
338 analysis. This identified the top molecules, pathways and master regulators that are different
339 between control and *Pelo*^{epiKO} samples.

340

341 **Polysome analysis**

342 Epidermal layers from WT and *Pelo*^{epiKO} were lysed as described above (see Library generation
343 for ribosome profiling). Clarified lysates were loaded on 10-50% sucrose gradients prepared in
344 polysome gradient buffer (20mM Tris-HCl [pH8], 150mM KCl, 5mM MgCl₂, 0.5mM DTT,

345 0.1mg/mL cycloheximide), and gradients were spun in an SW41-Ti rotor at 40,000 rpm for 3 hr
346 at 4°C. Gradients were fractionated using a Brandel Density Gradient Fractionation System.
347 Prior to RNA extraction, CLuc mRNA (NEB) was added in each fraction. RNA was extracted
348 using hot acidic phenol and cDNA was synthesized using iScript cDNA synthesis kit (Bio-Rad)
349 according to manufacturer's instructions. qPCR was carried out using iTaq Universal SYBR
350 Green Supermix (Bio-Rad). Relative mRNA abundances in indicated fractions were normalized
351 to CLuc mRNA to account for differences in RNA extraction efficiency among fractions, and
352 then calculated as fold changes normalized to 80S fractions. qPCR primers: CLuc Forward 5'-
353 GCTTCAACATCACCGTCATTG-3', CLuc Reverse 5'-CACAGAGGCCAGAGATCATTC-3',
354 Krt86 Forward 5'-AACAGAATGATCCAGAGGCTG-3', Krt86 Reverse 5'-
355 GCTCAGATTGGGTCACGG-3'.

356

357 **RNA-seq library preparation and analysis**

358 Primary epidermal cell suspension was prepared as previously described³⁹. Briefly, cells were
359 harvested from 3 months old 4-OHT treated *Pelo*^{fl/+}; *Lrig1*^{EGFP-CreERT2}, *Pelo*^{fl/+}; *Lgr5*^{EGFP-CreERT2},
360 *Pelo*^{fl/+}; *Lgr6*^{EGFP-CreERT2} control mice and *Pelo*^{fl/fl}; *Lrig1*^{EGFP-CreERT2}, *Pelo*^{fl/fl}; *Lgr5*^{EGFP-CreERT2},
361 *Pelo*^{fl/fl}; *Lgr6*^{EGFP-CreERT2} *Pelo* mut mice. Total epidermal population was FACS sorted for GFP+
362 cells on a BD FACSAriaII cell Sorter and 1000 GFP-high cells collected from each population
363 for RNA-seq. Library construction and the strategy for RNA-seq was performed using Smart-
364 seq2 method as reported previously⁴⁰. Fastq files of paired-end reads were uploaded to Galaxy
365 platform⁴¹ and aligned using STAR aligner⁴² to *Mus musculus* reference genome
366 (GRCm38/Mm10). BAM files were processed in R using "rnaseqGene" workflow⁴³. The data
367 were analysed using the edgeR package. Processed data were mined using IPA Ingenuity

368 Pathway Analysis (Qiagen). The datasets are deposited in GEO under accession number
369 GSE106246.

370

371 **Flow cytometry for measurement of cell size, cycle and protein synthesis *in vivo***

372 To analyse cell size by flow cytometry, epidermal cells were isolated as previously described³⁹.
373 Briefly, epidermis was enzymatically separated from dermis with thermolysin (Sigma, 0.25
374 mg/mL in PBS) overnight at 4°C. Epidermal sheets were processed into single cell suspensions
375 by incubation in DMEM (Gibco) containing DNase (Sigma, 250 µg/mL) for 20 min at 37°C
376 with shaking. Single cells were labelled according to standard procedures with anti- Integrin α6-
377 Alexa Fluor 647 or FITC (AbSource, 1:20) antibody. To assess the percentage of proliferating
378 epidermal cells, mice were injected with 500µg 5-ethynyl-2'-deoxyuridine (EdU; 2.5mg/mL in
379 PBS) intraperitoneally and back skin was harvested 2 hr later. Cells were isolated as described
380 above and single cell suspensions were stained with the Click-iT EdU Alexa Fluor 488 Flow
381 Cytometry Kit (Invitrogen) according to the manufacturer's suggestions. Cell cycle analysis was
382 performed on a BD LSR Fortessa cell analyser. Proliferating cells that had incorporated EdU
383 were detected in the FITC/Alexa Fluor 488 channel.

384

385 To measure protein synthesis *in vivo*, mice received an intraperitoneal injection of O-propargyl-
386 puromycin (OP-P) (Medchem Source or Thermo Fisher (C10459); 50 mg kg⁻¹ body mass; pH
387 6.4–6.6 in PBS). One hour later mice were euthanized and back and tail skin samples were
388 collected. Epidermal dissociation was performed as described above. The staining for detection
389 of protein synthesis was performed according to the manufacturer instructions (Click-iT Plus
390 OPP Protein Synthesis Assay Kit; Thermofisher Scientific). Samples from PBS-injected mice
391 were also stained for detection of protein synthesis and the fluorescence signal was used to

392 determine background labelling. Rates of protein synthesis were calculated as described
393 previously³. Briefly, OP-P signals were normalized to whole epidermis after subtracting
394 autofluorescence background. ‘Mean OP-Puro fluorescence’ reflected fluorescence values for
395 each cell population normalized to whole epidermis. Labelled cells were analysed on a BD
396 LSRFortessa cell analyser. All data were analysed using FlowJo software.

397

398 **Histology, epidermal wholemounts and imaging**

399 For paraffin sections, skin samples were fixed with 10% neutral buffered formalin overnight
400 before paraffin embedding. The tissues were sectioned and stained with haematoxylin and eosin
401 (H&E) and Herovici’s stain by conventional methods. For frozen sections, skin samples were
402 embedded on OCT (optimal cutting temperature compound; VWR), sectioned and fixed in 4%
403 PFA for 10 min before staining. Slides were mounted using ProLong Gold anti-fade reagent
404 containing DAPI (Life Technologies) as a nuclear counterstain. Images were acquired using a
405 Hamamatsu slide scanner and analysed using NanoZoomer software (Hamamatsu).

406 The epidermal wholemount labelling procedure was performed as described previously^{44,45}. In
407 brief, mouse tail was slit on the ventral side lengthways. Pieces (0.5x0.5 cm²) of skin were
408 incubated in 5 mM EDTA in PBS at 37 °C for 4 h. Epidermis was gently peeled from dermis as
409 an intact sheet in a proximal to distal direction, corresponding to the orientation of the hairs, and
410 then the epidermis was fixed in 4% paraformaldehyde (PFA; Sigma) for 1 h at room temperature.
411 Fixed epidermal sheets were washed in PBS and stored in PBS containing 0.2% sodium azide at
412 4° C.

413 Confocal image acquisition of stained wholemounts and skin sections were performed using a

414 Nikon A1 confocal microscope. Images were analysed using NIS Elements (Nikon Instruments
415 Inc.). Photoshop CS5 (Adobe image suite) was used to optimize the images globally for
416 brightness, contrast and colour balance.

417 **Rapamycin treatment**

418 Rapamycin (LC Laboratories, R5000) was dissolved in acetone. Rapamycin treatment groups
419 received topical applications of 500 μ l 0.2% Rapamycin on dorsal and tail skin. Vehicle
420 treatment group mice received an equal volume of acetone without rapamycin. Dorsal skin was
421 shaved before the day of treatment.

422

423 **Wound and TEWL assays**

424 Full-thickness wounds were made on the lower dorsal skin (5mm) or tail (2mm) using punch
425 biopsy (Stiefel) under analgesia and general anaesthesia. The hair on the back was shaved prior
426 to wounding. Wound closure was measured using a Vernier scale. Epidermal barrier function
427 was assessed by testing basal transepidermal water loss (TEWL) on the dorsal skin of mice using
428 a TEWAmeter (Courage and Khazaka, TM210). Measurements were collected for 15–20
429 seconds when TEWL readings had stabilized, at approximately 30 seconds after the probe collar
430 was placed on the dorsal skin.

431

432 **Antibodies**

433 Primary antibodies for wholemount and tissue sections were: chicken anti-Krt14 (Covance,
434 SIG2376, 1:500) or directly conjugated (AlexaFluor 555) Krt14 (LL002, in house, 1:200);
435 directly conjugated (AlexaFluor 488) Krt15 (LHK-15, in-house, 1:50); human anti-p63 (SCBT,
436 sc367333, 1:100); rabbit anti-filaggrin (Covance, PRB-417P, 1:100); mouse anti-FASN (SCBT,

437 sc48357, 1:100); rabbit anti-Ki67 (Novocastra, NCL-Ki67p, 1:500); rabbit anti-Ki67 (abcam,
438 ab16667, 1:500); rabbit anti- Phospho-S6 Ribosomal Protein (Ser235/236) (pS6K, Cell
439 signaling, 2211, 1:200); rabbit anti-P-Cadherin (Cell signaling, 2130, 1:200); rabbit anti-
440 Vimentin (Cell signaling, 5741s, 1:500); rabbit anti-K10 (Covance, PRB-159P, 1:500); FITC
441 conjugated rat anti-CD49f (Integrin α 6, Biolegend, 313606, 1:100); goat anti-Lrig1 (R&D
442 Systems, FAB3688G, 1:200); rabbit anti-Scd1 (Cell signaling, 2794s, 1:500); mouse anti-
443 involucrin (SY5, in-house, 1:500); mouse anti-Pankeratin (abcam, ab8068, 1:200); rat anti-CD34
444 (RAM34, Thermo Fisher, 14-0341-82, 1:200); Rabbit anti-Phospho-4EBP1 (Thr37/46) (Cell
445 Signalling, 236B4, 1:500) AlexaFluor (Life Technologies) dye-conjugated secondary antibodies
446 were used at 1:250 dilutions.

447

448 ***In vitro* knockdown, clonogenicity and skin reconstitution assay**

449 Primary human keratinocytes (strain km) were isolated from neonatal foreskin and cultured on
450 mitotically inactivated 3T3-J2 feeder cells in complete FAD medium, containing 1 part Ham's
451 F12 medium and three parts Dulbecco's modified Eagle's medium (DMEM), 10⁻⁴ M adenine,
452 10% (v/v) FBS, 0.5 μ g ml⁻¹ hydrocortisone, 5 μ g ml⁻¹ insulin, 10⁻¹ M cholera toxin and 10 ng
453 ml⁻¹ EGF, as described previously^{46,47}. siRNA mediated gene silencing was performed as
454 described previously⁴⁸. Briefly, keratinocytes were transferred to feeder free conditions in
455 keratinocyte serum-free medium (KSFM) containing 30 μ g ml⁻¹ BPE (bovine pituitary extract)
456 and 0.2 ng ml⁻¹ EGF (Gibco) for 2–3 days. Cells were trypsinized at ~70% confluence and
457 resuspended in cell line buffer SF (Lonza). For each 20 μ l transfection (program FF-113), 2 \times 10⁵
458 cells were mixed with 1–2 μ M siRNA duplexes (Silencer select siRNA for *PELO* ID131910,
459 ID131911, ID131912, as well as negative control, Ambion). Transfected cells were incubated at

460 room temperature for 5–10 min and subsequently resuspended in pre-warmed KSFM. siRNA
461 nucleofections were performed with the Amaxa 16-well shuttle system (Lonza). Alternatively,
462 keratinocytes cells were transfected by using INTERFERin (Polyplus transfections): 36pmol
463 siRNA, 4ul INTERFERin reagent, and 200ul KSFM were mixed in the collagen coated (20ug/ml
464 in PBS, 1h, 37°) 12-well plate and incubated 20min at room temperature. After the incubation,
465 75, 000 keratinocytes were seeded to the well (final concentration of siRNA 30nM). Medium
466 was changed after 4 hrs and cells were harvested after 48 hrs.

467
468 For clonogenicity assays, nucleofected keratinocytes were seeded at low density (100-250 cells
469 per well) on a prepared feeder layer in 6-well plates containing FAD medium. Keratinocytes
470 were maintained in culture for 12 days and then feeders were removed by Versene treatment
471 combined with tapping the culture flask. Once all the feeder cells were washed away, the
472 remaining keratinocytes colonies were fixed with 4% PFA at room temperature for 10 min.
473 Colonies were then stained with 1% Rhodanile Blue (1:1 mixture of Rhodamine B and Nile Blue
474 A (Acros Organics) solution for 15min and washed with distilled water prior to examination.
475 Stained dishes containing keratinocyte colonies were imaged using a Molecular Imager Gel Doc
476 XR+ imaging system (Bio-Rad). Colonies were measured using ImageJ and clonogenicity was
477 calculated as the percentage of plated cells that formed colonies.

478
479 For the skin reconstitution assay, pre-confluent keratinocyte cultures (KM passage 3) were
480 disaggregated and transfected either with *PELO* siRNAs or scrambled control siRNAs. 24 hours
481 post-transfection, keratinocytes were collected and reseeded on irradiated de-epidermised human
482 dermis in 6-well Transwell plates with feeders and cultured at the air–liquid interface for three

483 weeks⁴⁹. Organotypic cultures were fixed in 10% neutral buffered formalin (overnight), paraffin
484 embedded and sectioned for H&E and immunofluorescence analysis.

485
486 **Picrosirius birefringence and dermal thickness and cell density**

487 12µm paraffin sections were stained with picrosirius red using a standard method⁵⁰. Briefly, the
488 sections were de-paraffinized, washed twice with water and stained 1 hr in picrosirius red
489 solution (0.1% Sirius red F3B in saturated aqueous solution of picric acid). After the staining,
490 sections were washed twice with acidified water (0.5 % acetic acid), dehydrated, cleared with
491 xylene, and mounted with DPX mounting medium. The images were acquired using Zeiss
492 Axiophot microscope and AxioCam HRc camera under plane-polarized light. The quantification
493 of total collagen fibers was performed by Fiji (ImageJ) software. The collagen pixels were
494 selected by Color Treshold tool (Hue 0-100, Saturation 0-255 and Brightness 230-255).
495 Thickness of dermis was quantified by NanoZoomer Digital Pathology software (Hamamatsu).
496 The number of cells was determined with ImageJ by counting the nucleus in DAPI stained tissue
497 sections.

498
499 **Statistics**

500 Statistical significance in all experiments was calculated by Student's *t* test. Data are represented
501 as mean ±SEM (error bars). GraphPad Prism was used for calculation and illustration of graphs.

502
503 **Data Availability**

504 All experimental data generated during/and or analysed this study are included in this published
505 article (and its supplementary information files). In addition, ribosome profiling data (accession
506 number GSE94385) and RNAseq data (accession number GSE106246) are available in GEO.

507 **References cited in Methods**

- 508 32 Nyamsuren, G. *et al.* Pelota regulates the development of extraembryonic endoderm
509 through activation of bone morphogenetic protein (BMP) signaling. *Stem Cell Res* **13**, 61-
510 74, doi:10.1016/j.scr.2014.04.011 (2014).
- 511 33 Barker, N. *et al.* Identification of stem cells in small intestine and colon by marker gene
512 Lgr5. *Nature* **449**, 1003-1007, doi:10.1038/nature06196 (2007).
- 513 34 Snippert, H. J. *et al.* Lgr6 marks stem cells in the hair follicle that generate all cell
514 lineages of the skin. *Science* **327**, 1385-1389, doi:10.1126/science.1184733 (2010).
- 515 35 Madisen, L. *et al.* A robust and high-throughput Cre reporting and characterization
516 system for the whole mouse brain. *Nat Neurosci* **13**, 133-140, doi:10.1038/nn.2467
517 (2010).
- 518 36 Sosis, D., Richardson, J. A., Yu, K., Ornitz, D. M. & Olson, E. N. Twist regulates
519 cytokine gene expression through a negative feedback loop that represses NF-kappaB
520 activity. *Cell* **112**, 169-180 (2003).
- 521 37 Lichtenberger, B. M., Mastrogiannaki, M. & Watt, F. M. Epidermal beta-catenin
522 activation remodels the dermis via paracrine signalling to distinct fibroblast lineages. *Nat*
523 *Commun* **7**, 10537, doi:10.1038/ncomms10537 (2016).
- 524 38 Skarnes, W. C. *et al.* A conditional knockout resource for the genome-wide study of
525 mouse gene function. *Nature* **474**, 337-342, doi:10.1038/nature10163 (2011).
- 526 39 Jensen, K. B., Driskell, R. R. & Watt, F. M. Assaying proliferation and differentiation
527 capacity of stem cells using disaggregated adult mouse epidermis. *Nat Protoc* **5**, 898-911,
528 doi:10.1038/nprot.2010.39 (2010).
- 529 40 Picelli, S. *et al.* Full-length RNA-seq from single cells using Smart-seq2. *Nat Protoc* **9**,
530 171-181, doi:10.1038/nprot.2014.006 (2014).
- 531 41 Afgan, E. *et al.* The Galaxy platform for accessible, reproducible and collaborative
532 biomedical analyses: 2016 update. *Nucleic Acids Res* **44**, W3-W10,
533 doi:10.1093/nar/gkw343 (2016).
- 534 42 Dobin, A. *et al.* STAR: ultrafast universal RNA-seq aligner. *Bioinformatics* **29**, 15-21,
535 doi:10.1093/bioinformatics/bts635 (2013).
- 536 43 Love, M. I., Anders, S., Kim, V. & Huber, W. RNA-Seq workflow: gene-level
537 exploratory analysis and differential expression. *F1000Res* **4**, 1070,
538 doi:10.12688/f1000research.7035.1 (2015).
- 539 44 Braun, K. M. *et al.* Manipulation of stem cell proliferation and lineage commitment:
540 visualisation of label-retaining cells in wholemounts of mouse epidermis. *Development*
541 **130**, 5241-5255, doi:10.1242/dev.00703 (2003).
- 542 45 Liakath-Ali, K. *et al.* Novel skin phenotypes revealed by a genome-wide mouse reverse
543 genetic screen. *Nat Commun* **5**, 3540, doi:10.1038/ncomms4540 (2014).
- 544 46 Lowell, S., Jones, P., Le Roux, I., Dunne, J. & Watt, F. M. Stimulation of human
545 epidermal differentiation by delta-notch signalling at the boundaries of stem-cell clusters.
546 *Curr Biol* **10**, 491-500 (2000).
- 547 47 Gandarillas, A. & Watt, F. M. Changes in expression of members of the fos and jun
548 families and myc network during terminal differentiation of human keratinocytes.
549 *Oncogene* **11**, 1403-1407 (1995).
- 550 48 Mulder, K. W. *et al.* Diverse epigenetic strategies interact to control epidermal
551 differentiation. *Nat Cell Biol* **14**, 753-763, doi:10.1038/ncb2520 (2012).

552 49 Sen, G. L., Reuter, J. A., Webster, D. E., Zhu, L. & Khavari, P. A. DNMT1 maintains
553 progenitor function in self-renewing somatic tissue. *Nature* **463**, 563-567,
554 doi:10.1038/nature08683 (2010).
555 50 Lattouf, R. *et al.* Picrosirius red staining: a useful tool to appraise collagen networks in
556 normal and pathological tissues. *J Histochem Cytochem* **62**, 751-758,
557 doi:10.1369/0022155414545787 (2014).

558

559 **Supplementary Tables**

560 **Table S1:** List of specific keratins enriched for short footprints

561 **Table S2:** GO analysis of transcripts enriched in short ribosomal footprints. Genes enriched for
562 each GO category are presented in separate tabs.

563 **Table S3:** GO analysis of differentially expressed transcripts. Genes enriched for each GO
564 category are presented in separate tabs.

565

566 **Table S4:** List of differentially expressed genes among Lrig1+, Lgr5+, Lgr6+ control and Pelo-
567 mutant populations, intersections between Lrig1+, Lgr5+, Lgr6+ control and Pelo-mutant
568 populations.

569 **Table S5:** List of upstream regulators and canonical pathways activated in among and between
570 control Lrig1+, Lgr5+ and Lgr6+ subpopulations.

571

572

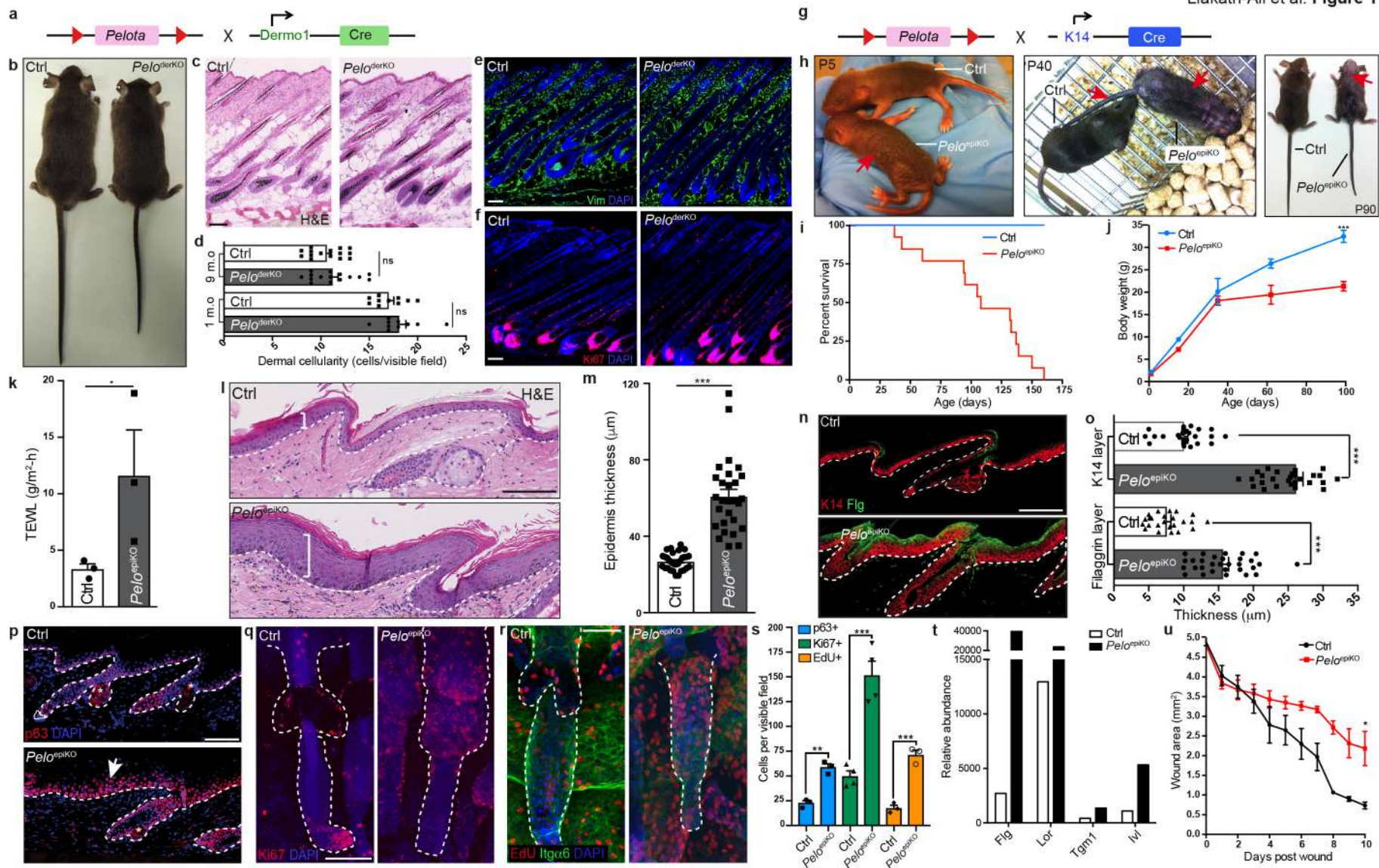


Fig. 1. Differential effects of *Pelo* deletion *Pelo*^{derKO} (a-f) and *Pelo*^{epiKO} (g-u) mice. (h) Arrows: skin abnormalities. (c, d, l, m) H&E staining of back (c, d) and tail (l, m) skin. Dermal cellularity (d) and epidermal thickness (m) were measured. n=2-4 sections from n=3 mice. (e, f, n, p-r) Immunolabelling of sections (e, f, n, p) and wholemounts (q, r). Asterisks: non-specific; arrow: suprabasal labelling; dashed lines: epidermal-dermal boundary. (m, n) ****p*<0.001, n=3 mice. (i) Kaplan-Meier curves (n=29 mice). (j) Body weight: ****p*<0.0003; n=5 per group. (k) TEWL. *p*<0.05; n=3. (s) Quantification of proliferation. ***p*=0.0086; ****p*=0.0003 for Ki67; 0.0006 for EdU; n=3. (t) Cumulative mean values of gene expression from ribosome profiling. (u) Wound closure. **p*=0.0500; n=3. Ctrl: littermate controls. Scale bars 100 μ m.

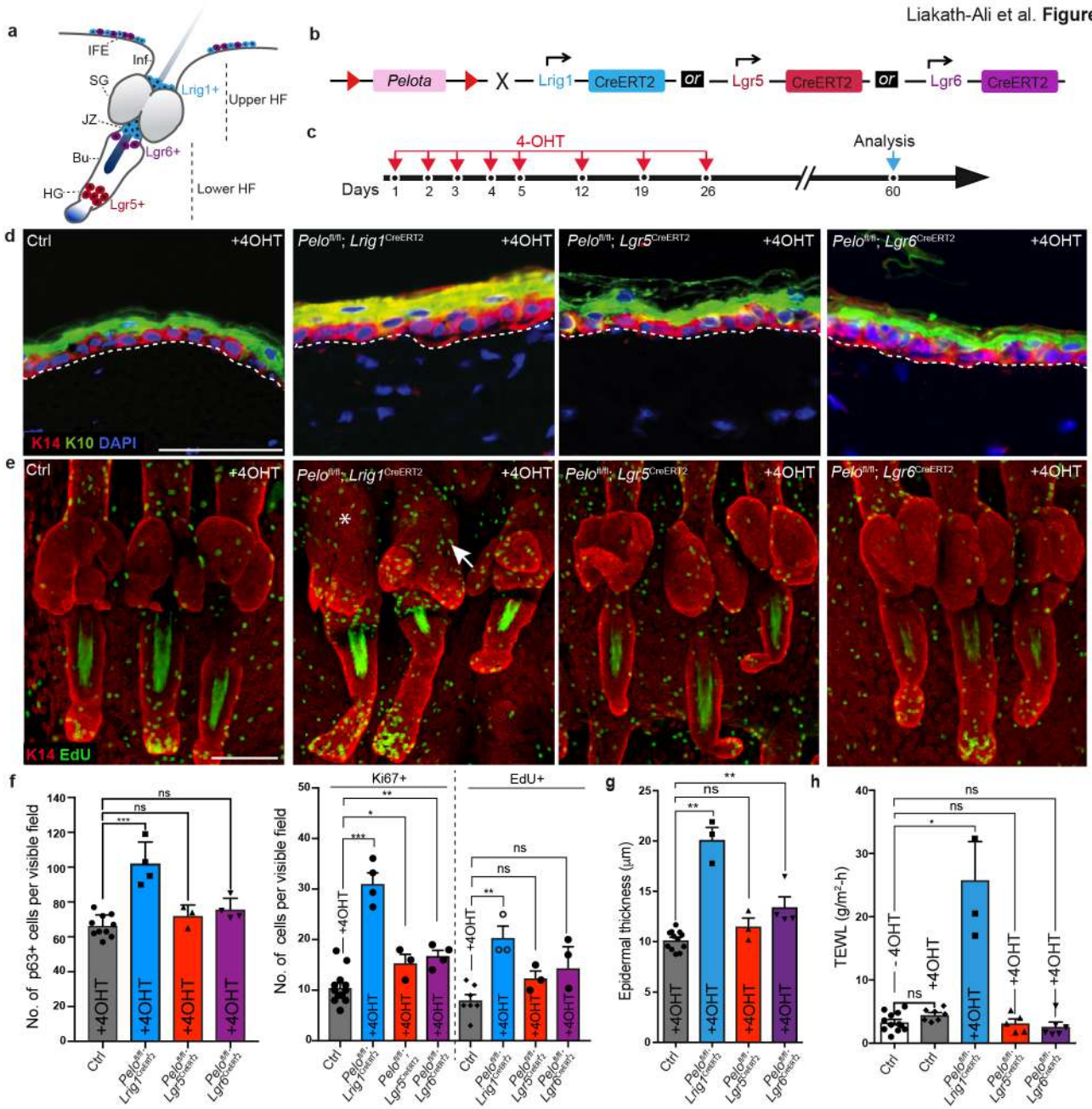


Fig. 2. Lrig1+ stem cells account for *Pelo* mutant epidermal phenotype (a-c) Schematics of *Lrig1*, *Lgr5* and *Lgr6* expression (a), breeding (b) and 4-OHT treatment (c). (d, e) Immunostaining of dorsal skin IFE sections (d) and tail wholemounts (e) with antibodies to the markers shown. (e) Asterisk: altered SG; arrow: altered JZ. (g-i) Quantification of proliferation (f), epidermal thickness (g) and TEWL (h). IFE, interfollicular epidermis; Inf, infundibulum; SG, sebaceous gland; JZ junctional zone; Bu, bulge; HG, hair germ. Scale bars 50 μm (d, f); 100 μm (e). Dashed lines: epidermal-dermal boundary. *** $p=0.0010$ (g, p63); *** $p=0.0005$; * $p=0.0330$, ** $p = 0.0071$ (g, Ki67); ** $p=0.0083$ (g, EdU). ** $p=0.0044$, 0.0011 (h). * $p=0.0167$ (i), $n = 3$ to 5 mice per group. n.s., non significant.

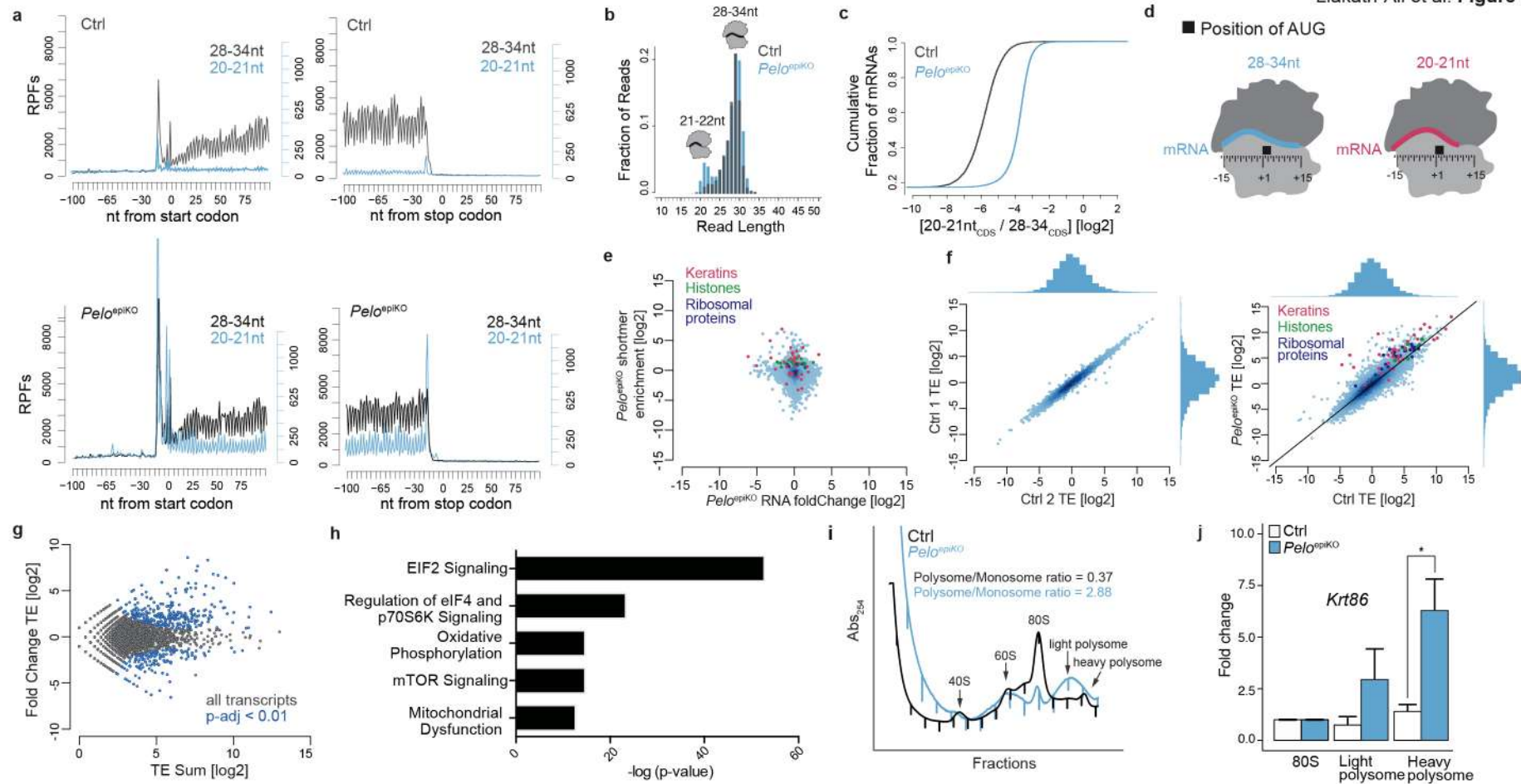


Fig. 3. Accumulation of short ribosome footprints and global translational changes in *Pelo* knockout epidermis (a) Metagene analysis of full length and short RPFs near the start (left) and stop (right) codons. (b) RPF read length distributions. (c) Empiric cumulative distribution plot of global enrichment of short 20-21nt relative to expected 28-34nt reads. (d) Designations of -15 peaks indicate positions of 5' end of RPF; corresponding P site occupancy shown. (e) Relative enrichment of short RPFs (y-axis) and change in RNA transcript levels (x-axis). (f) Replicate analysis of translational efficiency (TE). (g) MA plot showing observed and expected variance in TE measurements; p-adjusted <0.01, blue transcripts. (h) Canonical pathways linked to translation regulation in *Pelo*^{epiKO}. (i) Epidermal polysome profiling. (j) qRT-PCR shows significant increase in heavy polysome bound *Krt86* mRNA; $p=0.019$.

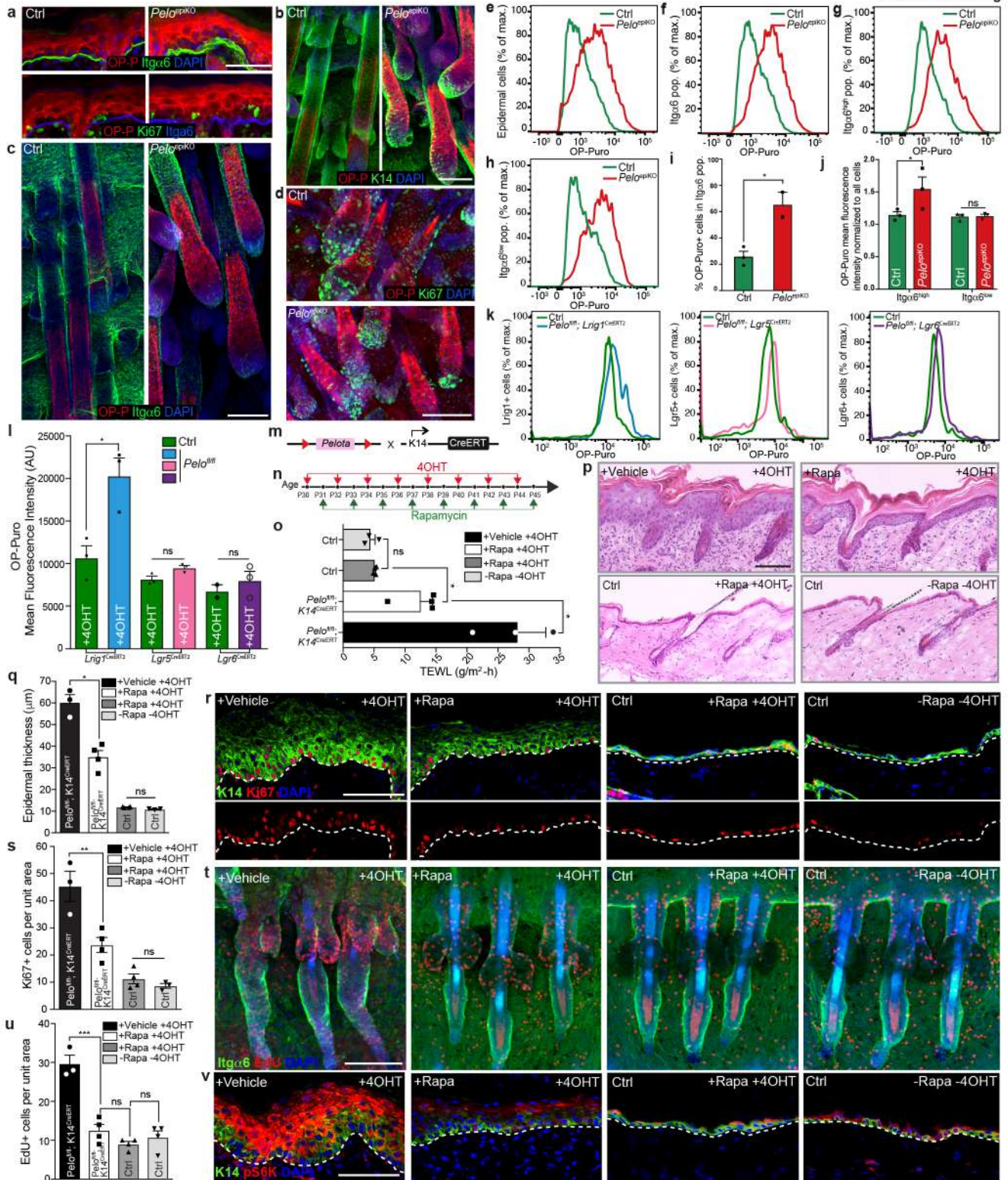


Fig. 4. Inhibition of mTOR pathway attenuates Pelo phenotype progression (a-d, r, t, v)
Immunolabelling for markers indicated. (s, u) Quantitation: ** $p=0.0064$ (s); *** $p=0.0006$ (u).
(b-l) OP-Puro injected newborn (b-j) and adult (k, l) mice. (e-k) Representative flow
histograms and (i, j, l) quantitation; $n=3$ mice per group. * $p=0.0406$ (i), 0.0357 (j), 0.0198 (l).
(m-v) 4-OHT and rapamycin (Rapa) treatment. (o) TEWL; * $p=0.0145$. (p, q) H&E stained
dorsal skin. * $p=0.0286$. Scale bars 50 μm (a); 100 μm (b-d; p, r, s, v), $n = 3-4$ mice per group.